

Crystal structure solution of a high-pressure polymorph of scintillating MgMoO_4 and its electronic structure

J. Ruiz-Fuertes ^{1,*}, A. Friedrich ², N. Garg ^{3,4}, V. Monteseuro ¹, K. Radacki ², D. Errandonea ⁵, E. Cavalli ⁶, P. Rodríguez-Hernández ⁷ and A. Muñoz ⁷

¹DCITIMAC, Universidad de Cantabria, Avenida Los Castros 48, 39005 Santander, Spain

²Institut für Anorganische Chemie, Julius-Maximilians-Universität Würzburg, 97074 Würzburg, Germany

³Homi Bhabha National Institute, Anushaktinagar, Mumbai 400 094, India

⁴High pressure and Synchrotron Radiation Physics Division, Bhabha Atomic Research Centre, Mumbai 400 085, India

⁵ICMUV, Departament de Física Aplicada, Universitat de València, Dr. Moliner 50, 46100 Burjassot, Spain

⁶Department of Chemical Sciences, Life and Environmental Sustainability, Parma University, 43124 Parma, Italy

⁷Departamento de Física and Instituto de Materiales y Nanotecnología, Universidad de La Laguna, San Cristóbal de La Laguna, 38201 Tenerife, Spain



(Received 20 May 2022; revised 20 July 2022; accepted 20 July 2022; published 8 August 2022)

The structure of the potentially scintillating high-pressure phase of $\beta\text{-MgMoO}_4$ ($\gamma\text{-MgMoO}_4$) has been solved by means of high-pressure single-crystal x-ray diffraction. The phase transition occurs above 1.5 GPa and involves an increase of the Mo coordination from fourfold to sixfold accommodated by a rotation of the polyhedra and a concomitant bond stretching resulting in an enlargement of the c axis. A previous high-pressure Raman study had proposed such changes with a symmetry change to space group $P2_1/c$. Here it has been found that the phase transition is isosymmetrical ($C2/m \rightarrow C2/m$). The bulk moduli and the compressibilities of the crystal axes of both the low- and the high-pressure phase, have been obtained from equation of state fits to the pressure evolution of the unit-cell parameters which were obtained from powder x-ray diffraction up to 12 GPa. The compaction of the crystal structure at the phase transition involves a doubling of the bulk modulus B_0 changing from 60.3(1) to 123.7(8) GPa and a change of the most compressible crystal axis from the $(0, b, 0)$ direction in $\beta\text{-MgMoO}_4$ to the $(0.9a, 0, 0.5a)$ direction in $\gamma\text{-MgMoO}_4$. The lattice dynamical calculations performed here on $\gamma\text{-MgMoO}_4$ served to explain the Raman spectra observed for the high-pressure phase of $\beta\text{-MgMoO}_4$ in a previous work demonstrating that the use of *internal modes* arguments in which the MoO_n polyhedra are considered as separate vibrational units fails at least in this molybdate. The electronic structure of $\gamma\text{-MgMoO}_4$ was also calculated and compared with the electronic structures of $\beta\text{-MgMoO}_4$ and MgWO_4 shedding some light on why MgWO_4 is a much better scintillator than any of the phases of MgMoO_4 . These calculations yielded for $\gamma\text{-MgMoO}_4$ a $Y_2\Gamma \rightarrow \Gamma$ indirect band gap of 3.01 eV in contrast to the direct bandgaps of $\beta\text{-MgMoO}_4$ (3.58 eV at Γ) and MgWO_4 (3.32 eV at Z).

DOI: [10.1103/PhysRevB.106.064101](https://doi.org/10.1103/PhysRevB.106.064101)

I. INTRODUCTION

The search for target-selective detectors for cryogenic detection of the double- β decay has spurred the study of metal tungstate and molybdate scintillators [1,2]. This family of compounds presents a unique phonon and scintillating response allowing the separate detection of both isolated events and their surrounding radioactive background [3,4]. However, the performance of both molybdates and tungstates is not always comparable. The bandgap of these compounds occurs between the oxygen $2p$ orbitals (valence band) and the molybdate/tungsten d orbitals (conduction band) [5]. Although so similar, the luminescence of tungstates usually presents a much higher quenching temperature than in molybdates even in isostructural compounds [6]. As an example, the double- β decay of ^{100}Mo could not be found with the supposedly best suited molybdate MgMoO_4 [1]. MgMoO_4

crystallizes either in triclinic [7] ($\alpha\text{-MgMoO}_4$, space group $P\bar{1}$) or in monoclinic [8] ($\beta\text{-MgMoO}_4$, space group $C2/m$) symmetry at ambient conditions. In both structures, Mo is tetrahedrally coordinated. In order to compare the luminescence efficiency between α - and β - MgMoO_4 with the highly efficient MgWO_4 (wolframite-type structure, space group $P2_1/c$), Mikhailik *et al.* [1] studied the $\text{MgW}_x\text{Mo}_{1-x}\text{O}_4$ solid solution. They found that while $\alpha\text{-MgMoO}_4$ has a Stokes shift of 2.05 eV, the Stokes shifts of $\beta\text{-MgMoO}_4$ and MgWO_4 are identical (~ 1.5 eV), leaving the explanation for the different luminescence efficiency open. The main difference between both compounds is their Mo/W coordination and, therefore, their electronic band structures. While Mo is tetrahedrally coordinated in all the known structures of MgMoO_4 , W is octahedrally coordinated in MgWO_4 and it has a better luminescence efficiency. In a high-pressure Raman spectroscopy study Coelho *et al.* [9] found a high-pressure polymorph of MgMoO_4 ($\gamma\text{-MgMoO}_4$), for which they proposed an octahedral coordination of Mo. Based on vibrational arguments they concluded that $\gamma\text{-MgMoO}_4$ might have the

*ruizfuertesj@unican.es

TABLE I. Details of the two high-pressure single-crystal x-ray data collections performed on MgMoO_4 .

	$\beta\text{-MgMoO}_4$	$\gamma\text{-MgMoO}_4$
p (GPa)	0.87(4)	1.95(10)
h	-16;16	-15;15
k	-15;14	-14;14
l	-5;3	-6;5
Observed refl.	656	649
Unique refl.	310	284
R_{int}	0.0492	0.0155

wolframite-type structure of MgWO_4 , which would add this high-pressure polymorph to the list of possible scintillators. Although the wolframite-type structure had been previously [10] proposed for MgMoO_4 at 0.6 GPa and 900°C, the crystal structure of $\gamma\text{-MgMoO}_4$ remained unsolved and, hence, its electronic structure remains unexplored.

In this work, we have determined the crystal structure of $\gamma\text{-MgMoO}_4$ using high-pressure single-crystal and powder x-ray diffraction (XRD). Subsequently, its lattice vibrations and electronic band structure were calculated by means of *ab initio* calculations. Finally, we have calculated the electronic structures of $\beta\text{-MgMoO}_4$ and MgWO_4 to compare them with that of $\gamma\text{-MgMoO}_4$.

II. EXPERIMENTAL DETAILS

In the single-crystal XRD (SXRD) experiments a Boehler-ALMAX diamond-anvil cell (DAC) with an opening angle of 70° and anvil culets of 500 μm in diameter was used for pressure generation. A stainless steel gasket pre-indented to 40 μm in thickness with a 200 μm diameter hole in the center served as the pressure chamber. A mixture of methanol-ethanol (4:1), hydrostatic up to 9 GPa [11] was used as a pressure-transmitting medium and a ruby chip was inserted to determine the pressure [12]. The sample of $\beta\text{-MgMoO}_4$ was cut from a large single crystal grown by the flux growth method [13]. The single crystal used had dimensions of 60 \times 40 \times 10 μm^3 and it was oriented along the exfoliation plane (001). The experiment was performed at the High-Pressure Diffraction beamline (ID15B) at the ESRF synchrotron employing a 5 \times 5 μm^2 collimated beam with a wavelength of 0.4117 Å. Data collections were performed at 0.87(4) and 1.95(10) GPa collecting the diffraction frames in ω steps of 0.5° along the opening range of the DAC. The indexation and intensity integration were carried out using the CrysAlis^{Pro} [14] software and the structure solution and refinement were carried out with the SHELXT [15] and SHELXL [16] programs, respectively, implemented in the SHELXLE user interface [17]. Details of the data collection are shown in Table I.

The powder XRD experiments were carried out at the BL11 beamline of the INDUS2 synchrotron source, employing a wavelength of 0.5026 Å up to pressures of 12 GPa while increasing and decreasing pressure. The data were collected using a MAR345 image plate detector. CeO_2 was used to determine the sample to detector distance (230 mm) and also to calibrate the detector parameters. The two-dimensional

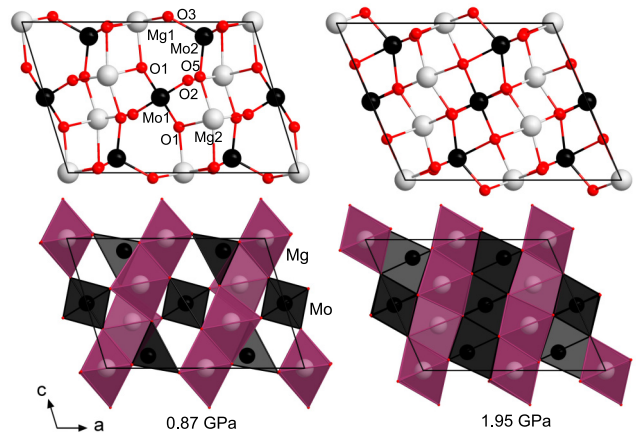


FIG. 1. Crystal structures of (left) $\beta\text{-MgMoO}_4$ at 0.87(4) GPa and (right) its high-pressure polymorph, $\gamma\text{-MgMoO}_4$ at 1.95(10) GPa, projected along the b axis. Top: ball-and-stick drawing; Mg, Mo, and O atoms are represented by gray, black, and red color, respectively. At the bottom, polyhedra drawing representing the coordination of Mg and Mo atoms by oxygen atoms.

diffraction images were converted to one-dimensional diffraction patterns using the FIT2D software. LeBail refinements were performed with the Fullprof program [18].

III. COMPUTATIONAL DETAILS

The stability of the high-pressure polymorph $\gamma\text{-MgMoO}_4$ determined from SXRD with respect to the structure of the β polymorph was tested and, subsequently, the lattice dynamics and electronic band structure of $\beta\text{-MgMoO}_4$, $\gamma\text{-MgMoO}_4$, and MgWO_4 were calculated with the Vienna *ab initio* simulation package (VASP) [19–21] using the density functional theory framework [22]. The pseudopotentials employed were the projector augmented wave [23] with a cutoff energy of 520 eV. The generalized gradient approximation was used with an AM05 functional [24,25] to describe the exchange-correlation energy. The Brillouin zone k -point integrations were performed using a 6 \times 6 \times 6 sampling for the primitive cell. Lattice-dynamics calculations were carried out with the PHONOPY [26] package that allows to obtain the eigenvalues and eigenvectors of the vibrational modes at the Γ point.

IV. RESULTS AND DISCUSSION

A. Structural solution

The crystal structure of the monoclinic ambient-pressure phase $\beta\text{-MgMoO}_4$ is shown on the left side of Fig. 1. It consists of ($\bar{1}01$) sheets of isolated MoO_4 tetrahedra sharing corners with MgO_6 octahedra, which are arranged in units of four edge-sharing octahedra within neighboring sheets. There exist two Mg and two Mo symmetry-independent positions. As explained above, Coelho *et al.* [9] found in a high-pressure Raman spectroscopy work that $\beta\text{-MgMoO}_4$ undergoes a structural phase transition at around 2 GPa which implies a frequency redistribution of most Raman active modes. Based on the concept of polyhedral internal modes

TABLE II. Lattice parameters a , b , c , β angle, unit-cell volume V , x , y , and z atomic coordinates, and isotropic thermal displacement U_{iso} of the crystal structures of β - and γ -MgMoO₄ at 0.87(4) and 1.95(10) GPa, respectively, obtained from single-crystal x-ray diffraction, and for comparison of γ -MgMoO₄ from calculations at a similar pressure of 2 GPa. The number of refined parameters, obtained residual values $R1$, $wR2$, and the Goodness of fit (GooF) are also shown. Space group $C2/m$, $Z = 8$. More details can be found in the crystallographic information file (CIF) files provided in the Supplemental Material [27].

	β -MgMoO ₄				γ -MgMoO ₄						
	Experimental 0.87(4) GPa				Experimental 1.95(10) GPa			Calculations 2 GPa			
a (Å)	10.2534(5)				9.6444(9)						
b (Å)	9.2594(1)				8.8283(1)						
c (Å)	7.016(2)				7.611(2)						
β (deg)	107.05(2)				113.73(2))						
V (Å ³)	636.8(2)				593.2(2)						
	x	y	z	U_{iso} (Å ²)	x	y	z	U_{iso} (Å ²)	x	y	z
Mo1	0.5	0.25061(7)	0.5	0.0065(3)	0.5	0.21397(6)	0.5	0.0180(11)	0.5	0.21413	0.5
Mo2	0.72947(10)	0.5	0.0959(4)	0.0062(3)	0.78543(10)	0.5	0.1399(3)	0.0153(12)	0.78563	0.5	0.14042
Mg1	0.5	0.1785(3)	0	0.0071(7)	0.5	0.1912(3)	0	0.0150(5)	0.5	0.19049	0
Mg2	0.7998(5)	0.5	0.6442(19)	0.0070(7)	0.8093(4)	0.5	0.6555(12)	0.0145(5)	0.80997	0.5	0.65603
O1	0.5413(7)	0.1537(5)	0.303(3)	0.0120(10)	0.4980(6)	0.1513(5)	0.2607(16)	0.0172(9)	0.49871	0.15022	0.26146
O2	0.3581(7)	0.3562(5)	0.387(3)	0.0184(12)	0.3467(6)	0.3347(4)	0.4239(17)	0.0200(9)	0.34510	0.33452	0.42317
O3	0.8595(9)	0.5	-0.036(4)	0.0062(13)	0.8473(9)	0.5	-0.066(2)	0.0160(11)	0.85002	0.5	-0.06094
O4	0.6334(7)	0.3441(6)	0.027(3)	0.0192(13)	0.6651(6)	0.3470(4)	0.0823(17)	0.0199(9)	0.66510	0.34523	0.08308
O5	0.3010(12)	0	0.363(4)	0.0206(19)	0.3497(10)	0	0.416(3)	0.0170(13)	0.54956	0.5	0.41486
Parameters	29				35						
$R1$ [$I > 2\sigma(I)$]	0.0354				0.0213						
$wR2$ (all data)	0.0912				0.0551						
GooF on F^2	1.086				1.156						

they concluded that (i) above 2 GPa Mo ions must be octahedrally coordinated and (ii) the high-pressure structure might be described either in $C2/m$ or $P2/c$ space groups, with $P2/c$ being the most probable. Though the reasoning is robust, the Raman spectroscopy study by Coelho *et al.* [9] leaves the structural solution of the high-pressure phase of MgMoO₄ as an open question.

We have solved the crystal structure of the high-pressure phase of MgMoO₄, γ -MgMoO₄, in space group $C2/m$. The crystal structure is shown in right side of Fig. 1, and the atomic coordinates of β -MgMoO₄ and γ -MgMoO₄ before and after the high-pressure phase transition, respectively, are given in Table II. The reconstruction of the reciprocal space obtained from the intensity data of γ -MgMoO₄ in our single-crystal XRD experiment at 1.95(10) GPa clearly confirms the presence of the C -face centered Bravais lattice by analysis of the systematic extinctions of reflection intensities and, hence, of the reflection conditions. Figure 2 shows sections of three reconstructed reciprocal layers, i.e., layers (a) $hk0$ and (b) $hk1$, which are projections along $[001]$, the c axis, and (c) $h0l$, which is a projection along $[010]$, the b axis. One can easily identify the reflection condition for the C -face centering as $h + k = 2n$ for all reflections hkl , occurring in all reciprocal layers. As a result, the space group of γ -MgMoO₄ is $C2/m$ and not, as previously proposed, $P2/c$, i.e., the structural phase transition is isosymmetric. The refinement of the determined crystal structure of γ -MgMoO₄ converged to an excellent agreement with small residual values of $R1 = 0.0213$ for reflections with $I > 2\sigma(I)$ and $wR2 = 0.0551$ for all reflections (Table II), which confirms the correctness

of our structural model and the selection of the proper space group. The obtained crystal structure is further confirmed by the excellent agreement between the observed and calculated powder XRD patterns at 5 GPa in the Rietveld refinement [Fig. 2(d)].

The phase transition is driven by the rotation of both MoO₄ tetrahedra, which concomitantly increase their coordination from 4 to 6 oxygen atoms. Mo1 forms two long bonds with O5 oxygen atoms [Mo1–O5 = 2.309(6) Å at 1.95(10) GPa], while Mo2 forms two bonds with O1 oxygen atoms of similar length (Mo2–O1 = 2.305(5) Å (Table S1 [27])). The formation of the MoO₆ octahedra is accompanied by a straightening of their O – Mo – O axes that are parallel to the c axis (Fig. 1). The rotation and coordination increase of the MoO₄ tetrahedra has an overall strong impact on the stretching of Mg – O – Mo chains that are oriented in the direction of the c axis. Along the one chain, by forming the Mo1O₆ octahedron, the O1–Mo1–O1 angle increases by 26° from ca. 120 to 146°, and the Mg1–O1–Mo1 angle increases by ca. 17° from 136 to 153° (Fig. 1 and (Table S1 [27])). Along the other distinct chain oriented parallel to the c axis, by forming the Mo2O₆ octahedron, the O3–Mo2–O5 angle increases by ca. 33° from 113 to 146°, and the Mg2–O3–Mo2 angle increases by ca. 34° from 120 to 154°. This straightening of chains is accompanied by an expansion of the c axis by around 8%. This expansion, however, is compensated by the contraction of the a and b axes resulting in an overall, discontinuous decrease of the unit cell volume at the first-order type phase transition (Fig. 4). In γ -MgMoO₄ the MoO₆ octahedra are strongly distorted with an octahedral quadratic

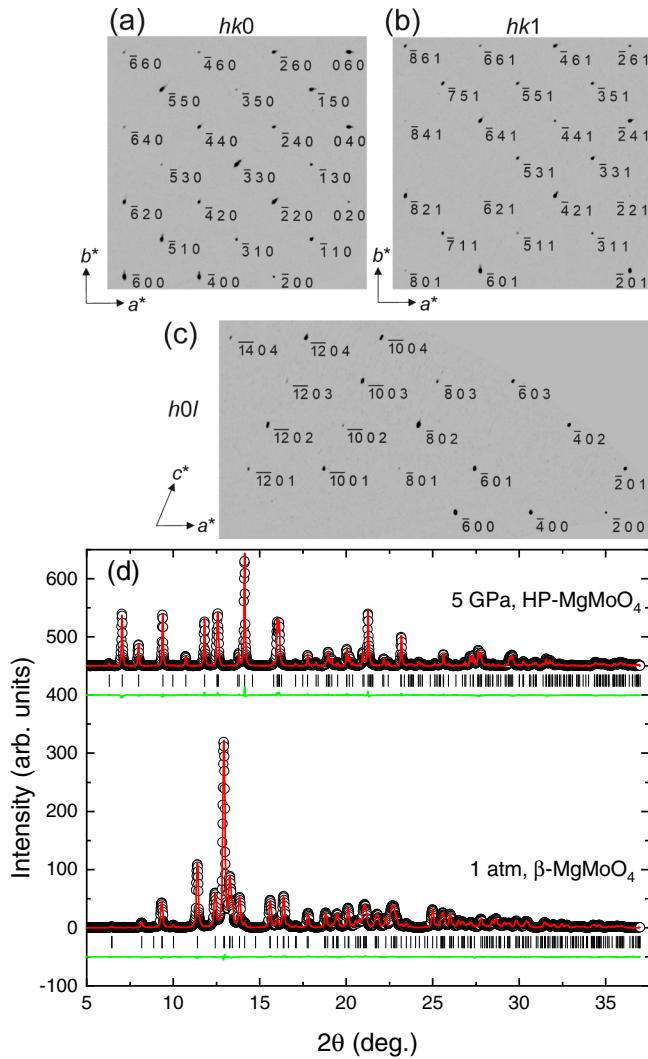


FIG. 2. Sections of the reciprocal space of γ -MgMoO₄ at 1.95(10) GPa in the (a) ($hk0$), (b) ($hk1$), and (c) ($h0l$) planes showing the reflection condition, i.e., $h + k = 2n$ for all reflections hkl , for the C-face centered Bravais lattice. (d) Powder XRD patterns of β -MgMoO₄ at 1 atm and of γ -MgMoO₄ at 5 GPa after the completion of the phase transition. Dots represent the experimental data while the red continuous lines are the Rietveld refinements. The 2θ location of the reflections and the residuals of the fit are also shown as vertical markers and continuous green lines, respectively.

elongation (OQE) [28] of ca. 1.065 and form units of four edge-sharing MoO₆ octahedra within the sheets, similarly to the arrangement of MgO₆ octahedra units in the neighboring sheets. Sheets are interconnected via common corners or edges. MgO₆ octahedra are much less distorted than MoO₆ octahedra in β -MgMoO₄ (OQE = 1.015) and become only slightly more distorted in γ -MgMoO₄ (OQE = 1.020) (Table S1 [27]). The crystal structure of γ -MgMoO₄ is isotypic to that of α -NiMoO₄ [29] indicating a reinterpretation of the previous high-pressure Raman spectroscopy study by Coelho *et al.* [9]. As explained above, Coelho *et al.* [9] conclude that the structure is a wolframite-type structure (space group $P2/c$) because the number of Raman internal modes of the Mo polyhedra changes from 8 to 6, which according to them could

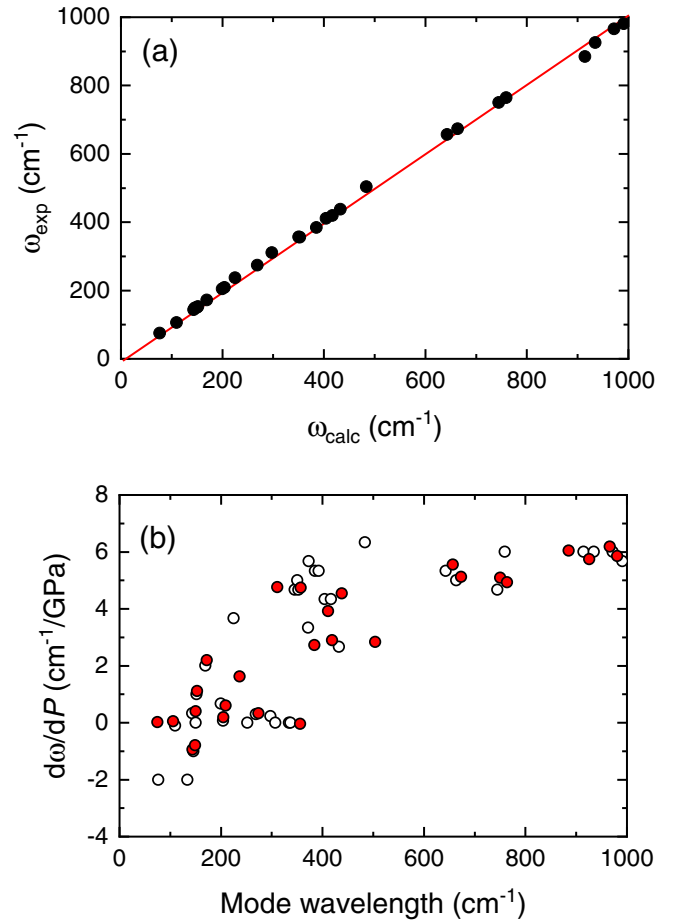


FIG. 3. (a) Experimental [9] ω_{exp} vs calculated ω_{calc} Raman frequencies of γ -MgMoO₄ show their excellent agreement. (b) Experimental [9] (open circles) and calculated (red dots) pressure coefficients of the same Raman active modes as a function of their frequencies.

only be explained with the Mo occupying a single MoO₆ octahedral site. However, even though our solved structure for γ -MgMoO₄ shows that Mo is octahedrally coordinated as suggested by Coelho *et al.* [9], the number of symmetry-independent positions for Mo is two (Table II).

B. Vibrational properties

In order to reevaluate the conclusions reached by Coelho *et al.* [9] we have performed *ab initio* lattice dynamic calculations with the solved structure of γ -MgMoO₄.

β -MgMoO₄ has 36 active Raman modes at zone center $\Gamma = 19A_g + 17B_g$, however, only 26 out of 36 modes can be observed experimentally [9].

According to our calculations, the solved structure for γ -MgMoO₄ becomes more stable than the β -MgMoO₄ phase above 1 GPa, in very good agreement with the experimental evidence found in our XRD studies and by Raman spectroscopy [9]. The comparison between the experimental and calculated Raman frequencies of the also 36 Raman active modes ($19A_g + 17B_g$) and their pressure coefficients are shown in Fig. 3(a). The calculated frequencies and their pressure coefficients can be found in Table S2 [27].

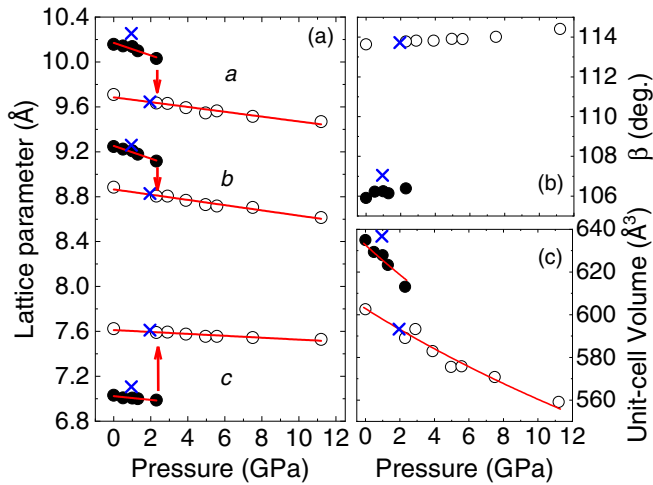


FIG. 4. (a) Pressure dependence of the lattice parameters of MgMoO₄. The arrows indicate the contraction of *a* and *b* as well as the expansion of *c*. (b) Pressure dependence of the monoclinic β angle. (c) Pressure dependence of the unit-cell volume of both phases. The full dots are data from the low-pressure β -MgMoO₄ phase while the empty dots are data from the high-pressure γ -MgMoO₄ phase. The straight lines are the fits to second-order Birch-Murnaghan equations of state.

The agreement between the experimental and the calculated frequencies is excellent with the experimental/calculated deviations within 2.5% [Fig. 3(a)]. The phonon gap of ~ 325 cm⁻¹ present in β -MgMoO₄ shrinks in γ -MgMoO₄ due to the coordination increase to sixfold coordination of the low-pressure tetrahedrally coordinated Mo ions (Table S1 [27]). This indicates that the experimental Raman spectrum of γ -MgMoO₄ [9] is very well described by our solved structure. Furthermore, in Fig. 3(b) we compare the experimental and calculated pressure coefficients $d\omega/dp$ of the Raman active modes of γ -MgMoO₄. Although in this case, the deviations for some modes are large, in general, the trend is followed with the low-frequency modes either softening or barely changing with frequency, and the high-frequency modes rapidly hardening under compression with pressure coefficients of ~ 6 cm⁻¹ GPa⁻¹. For the high-pressure phase the 36 Raman active modes can be observed experimentally probably due to the spreading in frequency of the modes as the result of the frequency gap disappearance which facilitates the modes detection with Raman spectroscopy.

These results show that the Raman spectrum found by Coelho *et al.* [9] above the structural phase transition can be explained by our γ -MgMoO₄ structure, highlighting that the intricate eigenvectors of the high-frequency modes cannot be simplified by considering the MoO₆ polyhedra as isolated blocks in which each mode involves a single Mo-O bond.

C. Compressibility

The pressure dependence of the unit-cell lattice parameters and volume of the two phases of MgMoO₄ is shown in Fig. 4.

The phase transition is detected at 2.28(5) GPa using powder XRD and at 1.95(10) GPa using SXRD, ca. 0.3 GPa higher

TABLE III. Calculated band gaps E_g for β -MgMoO₄, γ -MgMoO₄, and MgWO₄.

		Indirect E_g (eV)	Direct E_g (eV)
β -MgMoO ₄	$C_2 \rightarrow \Gamma$	3.56	Γ 3.58
γ -MgMoO ₄	$Y_2\Gamma \rightarrow \Gamma$	3.01	
MgWO ₄	$Y_2 \rightarrow Z$	3.23	Z 3.32

pressure than in previous Raman spectroscopy experiments [9] performed using the same pressure transmitting medium. The first-order character of the phase transition is evidenced by a unit-cell volume collapse of $\sim 5\%$ [Fig. 4(c)] and the irreversibility of the phase transition which was observed by Coelho *et al.* [9]. As explained above, the structural phase transition is the result of a stretching along the *c* axis of every three Mo-O-Mg chains, which results in an elongation of the *c* axis of $\sim 8\%$ [Fig. 4(a)]. In order to accommodate such a pressure-induced expansion, the other two axes decrease by $\sim 4\%$ and the monoclinic β angle increases by $\sim 7\%$ [Fig. 4(b)] producing the overall volume collapse. The pressure dependence of the unit-cell volumes of both phases can be fit with two second-order Birch-Murnaghan equations of state [Fig. 4(c)]. The obtained bulk moduli B_0 are 60.3(1) and 123.7(8) GPa for the β -MgMoO₄ and the γ -MgMoO₄ phases, respectively. Hence, the compaction of the structure at the phase transition (Fig. 1) results in a drastic increase of the incompressibility; the bulk modulus doubles its value. The change in compressibility observed in the volume reflects on the three monoclinic axes as observed in Fig. 4. While the incompressibility ($\kappa_x = -\frac{1}{x} \frac{\partial x}{\partial p}$) of the *a* and *b* axes changes from ~ 0.006 GPa⁻¹ in the low-pressure structure to ~ 0.002 GPa⁻¹ in the high-pressure structure, in the case of the *c* axis it changes from ~ 0.002 GPa⁻¹ to ~ 0.001 GPa⁻¹. Nevertheless, since the monoclinic angle of both structures is strongly deviating from 90°, the main axes of the strain ellipsoid can deviate a lot from the unit-cell axes [31]. In fact, while the highest compressibility in the β -MgMoO₄ is found in the X_2 crystal axis which coincides with the [0, *b*, 0] direction, in the γ -MgMoO₄ the highest compressibility, is on the *ab* plane along the [0.9*a*, 0, 0.5*c*] direction (crystal axis X_1).

D. Electronic band structure

Once the structure of γ -MgMoO₄ was solved, we computed its electronic band structure, which is shown in Fig. 5 in comparison with the electronic band structures of β -MgMoO₄ and MgWO₄ [30].

The electronic band structures of β -MgMoO₄, γ -MgMoO₄, and MgWO₄ show that their band gaps are indirect. In the case of γ -MgMoO₄ there is no apparent close direct band gap. However, in the case of β -MgMoO₄ and MgWO₄ the direct band gaps, the only observable experimentally, are 0.0153 eV at Γ (β -MgMoO₄) and 0.089 eV at Z (MgWO₄) wider than their indirect band gaps (Table III). Since both β -MgMoO₄ and MgWO₄ have indirect band gaps, the nature of their band gaps cannot be the cause of their different scintillating output. In fact, by looking at the electronic band

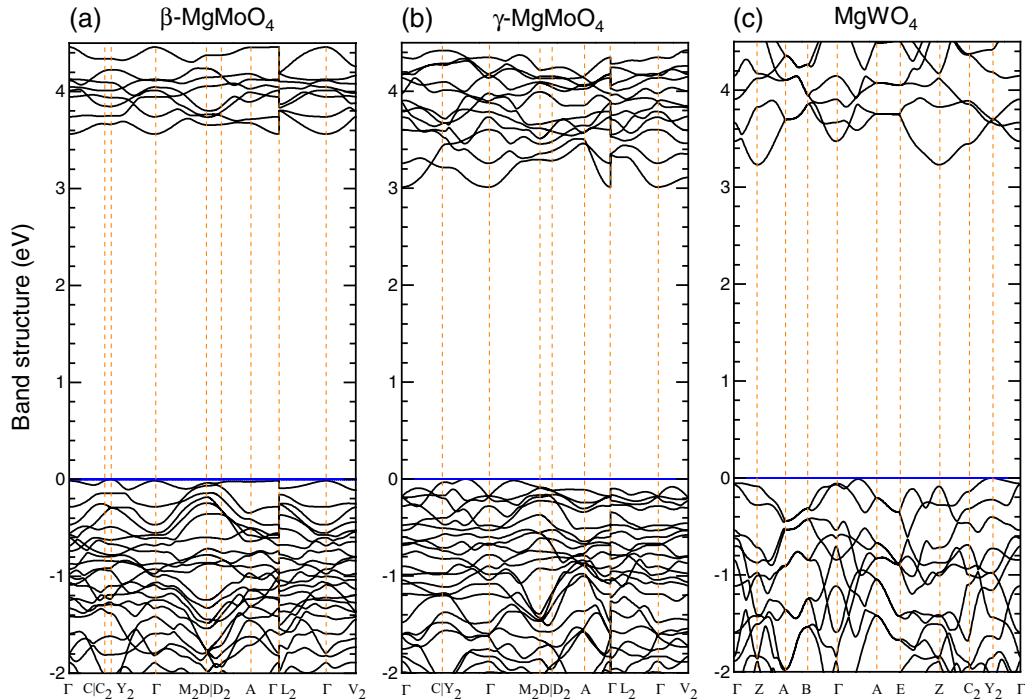


FIG. 5. Electronic structure of (a) β -MgMoO₄, (b) γ -MgMoO₄, and (c) MgWO₄. The last one was previously calculated [30]. The straight blue lines indicate the Fermi level.

structure of γ -MgMoO₄, despite of a coordination increase of Mo, the fully indirect band gap discards this polymorph for its use as a scintillator. Hence, the question arises, what the reason for such a poor scintillating output for β -MgMoO₄ might be.

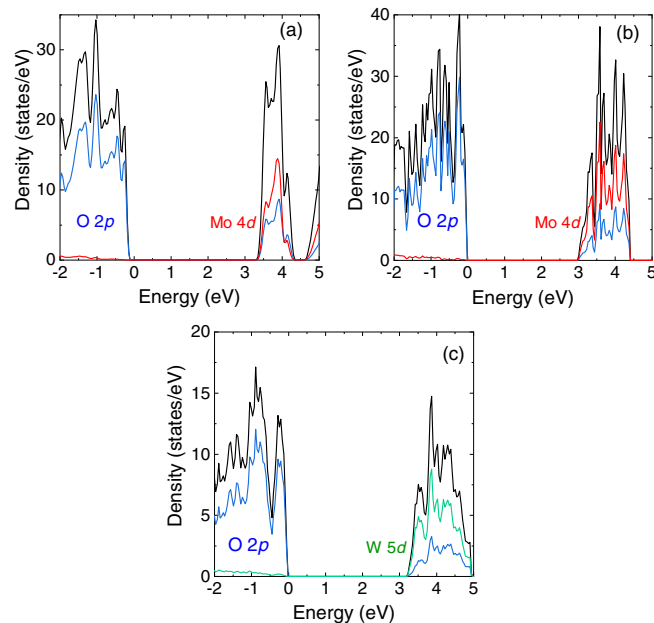


FIG. 6. Total (black) and partial (colors) density of states of the valence and conduction bands around the band gap showing the contribution of the different atomic orbitals in (a) β -MgMoO₄, (b) γ -MgMoO₄, and (c) MgWO₄.

The band gap of the three compounds is controlled (Fig. 6) by the O *p* and the Mo/W *d* orbitals since the Mg *s* orbitals are away from the maximum of the valence band or the minimum of the conduction band [30]. This configuration produces in the two compounds lowly dispersed and flat bands overall at the conduction band due to the high *d* character. A larger number of atoms occupying nonequivalent positions gives rise to a larger number of accessible electronic levels and therefore a higher density of states. Mo occupies two nonequivalent sites in both phases of MgMoO₄ while W is in a single site in MgWO₄. Therefore, MgMoO₄ is expected to have more electronic levels per eV at the conduction band and therefore a higher density of states. Both points can be visualized in Figs. 5 and 6 where the electronic band structure and density of states of MgMoO₄ (a) and (b) are compared with those of MgWO₄ (c). A larger number of accessible states can result into an increase of the energy transfer channels and therefore into a larger number of nonradiative decay mechanisms leading to a poor luminescence. This is similar to what occurs in extrinsic luminescence when the concentration of the luminescent ions is increased [32]. This hypothesis might explain why β -MgMoO₄ is a worse scintillator than MgWO₄.

V. CONCLUSIONS

The crystal structure of the high-pressure phase of β -MgMoO₄, i.e., γ -MgMoO₄, has been solved from high-pressure single-crystal x-ray diffraction data. The phase transition involves a compaction of the structure by a rotation of the polyhedra and a stretching of every three Mo-O-Mg bonds along the *c* axis that results in an increase of the Mo coordination from 4 to 6 and an elongation of the *c* axis. Interestingly, the phase transition is isosymmetric keeping two

symmetry-independent sites for Mo in contrast to what had been previously proposed in a high-pressure Raman spectroscopy work. At the onset of the phase transition at 1.5 GPa the unit-cell volume irreversibly contracts by 5%, and the bulk modulus doubles from 60.3(1) GPa to 123.7(8) GPa. On the basis of the crystal structure solution of γ -MgMoO₄ we have performed lattice dynamical and electronic band structure calculations, which find the high-pressure structure more stable above 1 GPa and have helped to explain the Raman spectrum observed previously for this phase and to compare its electronic band structure with that of β -MgMoO₄ and MgWO₄. The results here presented show that both polymorphs of MgMoO₄ are less efficient scintillators than MgWO₄. We explain this as: the results of the presence of a higher number of accessible states at the conduction band in the molybdates than in the tungstate. This produces an increase of the energy transfer channels which probably increases the probability of nonradiative emission of the excited electrons. In addition, we have found that γ -MgMoO₄ would even be a worse scintilla-

tor than β -MgMoO₄ since differently from β -MgMoO₄ and MgWO₄, its band gap of 3.01 eV is indirect ($Y_2\Gamma \rightarrow \Gamma$).

ACKNOWLEDGMENTS

The authors thank I. Collings and M. Handfland from the ID15B beamline at the ESRF for their help during the experiments, and O. Gomis from the Universitat Politècnica de València for the discussions. Most of the work presented in this work benefited from the financial support from the Spanish Ministerio de Ciencia e Innovación (MICINN) under Projects No. PID2019-106383GB-C41/43 (MCIN/AEI/10.13039/501100011033), MALTA Consolider-Team network RED2018-102612-T (MINECO/AEI/10.13039/501100003329), and from the Generalitat Valenciana under Project PROMETEO/2018/123. V.M. also thanks the MICINN for the Beatriz Galindo distinguished researcher program (BG20/00077).

-
- [1] V. B. Mikhailik, H. Kraus, V. Kapustyanyk, M. Panasyuk, Y. Prots, V. Tsybul'skyi, and L. Vasylechko, *J. Phys.: Condens. Matter* **20**, 365219 (2008).
- [2] D. A. Spasskii, V. N. Kolobanov, V. V. Mikhailin, L. Y. Berezovskaya, L. I. Ivieva, and I. S. Voronina, *Opt. Spectrosc.* **106**, 556 (2009).
- [3] S. Pirro, C. Anarboldi, J. W. Beeman, and G. Pessina, *Nucl. Instrum. Methods Phys. Res., Sect. A* **559**, 361 (2006).
- [4] P. de Marcillac, N. Coron, G. Dambier, J. Leblanc, and J.-P. Moalic, *Nature (London)* **422**, 876 (2003).
- [5] V. Monteseuro, J. Ruiz-Fuertes, J. Contreras-García, P. Rodríguez-Hernández, A. Muñoz, and E. Errandonea, *Appl. Phys. Lett.* **115**, 012102 (2019).
- [6] J. A. Groenik, C. Hakfoort, and G. Blasse, *Phys. Status Solidi A* **54**, 329 (1979).
- [7] S. C. Abrahams and J. M. Reddy, *J. Chem. Phys.* **43**, 2533 (1965).
- [8] P. Cord, P. Courtine, G. Pannetier, and J. Guillermet, *Spectrochimica Acta Part A* **28**, 1601 (1972).
- [9] M. N. Coelho, P. T. C. Freire, M. Maczka, C. Luz-Lima, G. D. Saraiva, W. Paraguassu, A. G. Souza Filho, and P. S. Pizani, *Vib. Spectrosc.* **68**, 34 (2013).
- [10] A. P. Young and C. M. Schwartz, *Science* **141**, 348 (1963).
- [11] R. J. Angel, M. Bujak, J. Zhao, G. D. Gatta, and S. D. Jacobsen, *J. Appl. Crystallogr.* **40**, 26 (2007).
- [12] H. K. Mao, J. Xu, and P. M. Bell, *J. Geophys. Res.* **91**, 4673 (1986).
- [13] E. Cavalli, A. Belletti, and M. G. Brik, *J. Phys. Chem. Solids* **69**, 29 (2008).
- [14] R. O. Diffraction, CrysAlis^{Pro} software system, version 1.171.38.43, Rigaku Corporation, Wroclaw, Poland (2015).
- [15] G. M. Sheldrick, *Acta Crystallogr., Sect. A: Found. Adv.* **71**, 3 (2015).
- [16] G. M. Sheldrick, *Acta Crystallogr. C: Struct. Chem.* **71**, 3 (2015).
- [17] C. B. Hübschle, G. M. Sheldrick, and B. Dittrich, *J. Appl. Crystallogr.* **44**, 1281 (2011).
- [18] J. Rodríguez-Carvajal, *Phys. B* **192**, 55 (1993).
- [19] G. Kresse and J. Hafner, *Phys. Rev. B* **47**, 558 (1993).
- [20] G. Kresse and J. Hafner, *Phys. Rev. B* **49**, 14251 (1994).
- [21] G. Kresse and J. Furthmüller, *Phys. Rev. B* **54**, 11169 (1996).
- [22] P. Hohenberg and W. Kohn, *Phys. Rev.* **136**, B864 (1964).
- [23] P. E. Blöchl, *Phys. Rev. B* **50**, 17953 (1994).
- [24] P. Armiento and A. E. Mattsson, *Phys. Rev. B* **72**, 085108 (2005).
- [25] A. E. Mattsson and R. Armiento, *Phys. Rev. B* **79**, 155101 (2009).
- [26] A. Togo and I. Tanaka, *Scr. Mater.* **108**, 1 (2015).
- [27] See Supplemental Material at <http://link.aps.org/supplemental/10.1103/PhysRevB.106.064101> for details on the crystal structure refinement, a table with the bond distances and a second table with the calculated and experimental phonon frequencies.
- [28] K. Robinson, G. V. Gibbs, and P. H. Ribbe, *Science* **172**, 567 (1971).
- [29] H. Ehrenberg, I. Svoboda, G. Witschek, M. Wiesmann, F. Trouw, H. Weitzel, and H. Fuess, *J. Magn. Magn. Mater.* **150**, 371 (1995).
- [30] J. Ruiz-Fuertes, S. López-Moreno, J. López-Solano, D. Errandonea, A. Segura, R. Lacomba-Perales, A. Muñoz, S. Radescu, P. Rodríguez-Hernández, M. Gospodinov *et al.*, *Phys. Rev. B* **86**, 125202 (2012).
- [31] M. J. Cliffe and A. L. Goodwin, *J. Appl. Crystallogr.* **45**, 1321 (2012).
- [32] V. Monteseuro, V. Venkatramu, U. R. Rodríguez-Mendoza, and V. Lavín, *Dalton Trans.* **50**, 9512 (2021).